

RSC Advances



This is an *Accepted Manuscript*, which has been through the Royal Society of Chemistry peer review process and has been accepted for publication.

Accepted Manuscripts are published online shortly after acceptance, before technical editing, formatting and proof reading. Using this free service, authors can make their results available to the community, in citable form, before we publish the edited article. This *Accepted Manuscript* will be replaced by the edited, formatted and paginated article as soon as this is available.

You can find more information about *Accepted Manuscripts* in the [Information for Authors](#).

Please note that technical editing may introduce minor changes to the text and/or graphics, which may alter content. The journal's standard [Terms & Conditions](#) and the [Ethical guidelines](#) still apply. In no event shall the Royal Society of Chemistry be held responsible for any errors or omissions in this *Accepted Manuscript* or any consequences arising from the use of any information it contains.

Cite this: DOI: 10.1039/c0xx00000x

www.rsc.org/xxxxxx

ARTICLE TYPE

One-pot template-free synthesis of heterophase BiVO₄ microspheres with enhanced photocatalytic activity

Yin Hu,^{a,b} Danzhen Li,^{*b} Fuqian Sun,^a Huibin Wang,^a Yaqing Weng,^a Wei Xiong^a and Yu Shao^b

Received (in XXX, XXX) Xth XXXXXXXXX 20XX, Accepted Xth XXXXXXXXX 20XX

DOI: 10.1039/b000000x

One-pot template-free hydrothermal method was developed for the fabrication of BiVO₄ microsphere with tetragonal-monoclinic heterophase structure. XRD and HRTEM characterizations confirmed the formation of heterophase structure. It was found that the molar ratio of Bi/V and hydrothermal time were critical parameters in the yield of the spherical morphology and heterophase structure. Benefiting from the unique morphology and existence of heterophase, the as-prepared BiVO₄ microsphere exhibited improved efficiency for RhB degradation in comparison with pure monoclinic scheelite-type BiVO₄ and tetragonal zircon-type BiVO₄. EPR and PL-TA techniques proved that the photoinduced active species were involved in the photocatalytic degradation of RhB. The enhanced photocatalytic performance can be attributed to the more effective separation of photogenerated carriers generated in the heterophase BiVO₄ system, as evidenced by the electrochemical measurement.

1. Introduction

TiO₂-based heterogeneous photocatalysis has been intensively investigated for the elimination of a variety of toxic chemicals.¹⁻³ However, TiO₂ can only utilize the photons in the UV region due to its wide band gap (3.2 eV), which limits its possibility of employing visible light. To increase the photo-efficiency of TiO₂ under visible light, a great deal of attention is directed towards the modification of TiO₂ and the exploration of visible-light-driven photocatalysts.⁴⁻⁷ Bismuth vanadate (BiVO₄), as one of the most promising non-TiO₂ based photocatalysts, has been proven to have a good photocatalytic activity under visible light for organic molecule degradation such as rhodamine B (RhB) and also for O₂ evolution.⁸ However, its practical applications are limited because of the poor electrical conductivity and the low separation efficiency of photogenerated electrons and holes.⁹ As a result, a number of approaches have been developed to improve the photocatalytic activity of BiVO₄, including doping with metal/nonmetal atoms,^{10,11} forming heterojunction structures,¹²⁻¹⁵ reducing the size of BiVO₄ and controlling the morphology and phase structure of BiVO₄.¹⁶⁻¹⁸ As we know, the photocatalytic activity of BiVO₄ is highly relevant to its crystal phase. BiVO₄ exists mainly in three crystalline phases: tetragonal scheelite, monoclinic scheelite and tetragonal zircon.¹⁹ Among the three polymorphs, the tetragonal zircon-structured BiVO₄ (z-t BiVO₄) is least investigated and inactive compared with the comprehensively studied monoclinic scheelite BiVO₄ (s-m BiVO₄). Thus, one can tune BiVO₄ from inert to highly reactive, simply by means of controlling the phase composition. The formation of surface phase junctions has been demonstrated as an effective strategy for improving the

photocatalytic efficiency. For instance, it is well-known that commercially available Degussa P25 TiO₂ (80% anatase and 20% rutile) is widely used as a benchmark model photocatalyst due to its high activity. Researchers have found that the crystallized rutile layer growing on the surface of anatase greatly promotes the separation of photogenerated charge carriers. The work by Li et al. verified that the phase junction formed between the surface anatase nanoparticles and rutile particles could greatly enhance the photocatalytic activity for photocatalytic H₂ production.²⁰ Besides TiO₂-based materials, they also found that the tailored α - β phase junctions on the surface of Ga₂O₃ significantly enhanced the photocatalytic activity for water splitting.²¹ And the transient absorption spectra further demonstrated the enhanced photocatalytic efficiency was ascribed to the efficient charge separation and transfer across the α - β phase junction.

Up to now, the search for such heterophase structured photocatalysts has focused mainly on UV light responsive catalysts.^{22,23} Visible light active photocatalyst with heterophase structure has seldom been reported. He et al. prepared α -Fe₂O₃/ γ -Fe₂O₃ heterophase nanorods by a facile thermal decomposition and redox method.²⁴ The material presented better visible-light photocatalytic performance than the single-phase α -Fe₂O₃ or γ -Fe₂O₃, suggesting that the well-structured interfaces and suitable band configuration were of great importance for enhancing its activity. More recently, Wang et al. found that a tight interface junction had been formed between BiVO₄ (s-m) and BiVO₄ (z-t) in a nanosize level.²⁵ Such a heterophase junction could promote electron migration across the interface, which accelerated the separation of photoinduced electron-hole pairs and obtained an increased photocatalytic activity. However, in the above studies, the heterophase materials were synthesized under relatively harsh conditions, such as high temperature, high pressure and multiple

steps. Hence, a facile, energy-saving and environmental-friendly method was desirable for achieving the successful fabrication of heterophase semiconductor photocatalysts.

In the present paper, we developed a one-pot additive-free hydrothermal method to prepare BiVO₄ microsphere with z-t & s-m heterophase structure. The effect of hydrothermal temperature, holding time and Bi/V molar ratio in the starting materials were described in detail. The obtained samples were characterized by XRD, FESEM, HRTEM and UV-vis DRS. Subsequently, the photocatalytic activity of the sample was evaluated for the liquid-phase photocatalytic degradation of RhB under visible light irradiation ($\lambda > 420$ nm). To deeply understand the mechanism of heterophase system, special attention was paid to the investigation of the active species involved in the photocatalytic process. This work has scientific significance and gives a better understanding about the crystal phase of BiVO₄ and its role in the photocatalytic activity. Our studies would provide a possible strategy to develop highly active photocatalysts by designing and preparing the heterophase junctions.

2. Experimental section

2.1 Synthesis

All chemicals used were analytic grade reagents without further treatments. In a typical procedure, 0.02 mol of Bi(NO₃)₃·2H₂O was firstly dissolved into 20 mL of concentrated nitric acid with continuous stirring for 2 h. A certain amount of NH₄VO₃ with different Bi/V molar ratio was added to 20 mL of 6 M NaOH aqueous. Then, the NH₄VO₃ aqueous solution was added to the Bi(NO₃)₃·2H₂O solution to form a homogeneous mixture, which was subsequently dropped to the 30 mL of 6 M NaOH aqueous slowly. Plenty of colorful precipitation appeared immediately after the addition. The resulting precursor was stirred for 2 h and then transferred into a Teflon-lined stainless steel autoclave of 100 mL capacity. The autoclave was sealed and maintained at 180 °C for different holding time and then cooled down naturally. Finally, the products were collected by filtration, washed several times with deionized water and absolute alcohol, and dried at 60 °C for 8 h.

2.2 Characterizations

The X-ray diffraction (XRD) patterns of the synthesized catalysts were performed using a Bruker D8 Advance X-ray diffractometer at 40 kV and 40mA with Ni-filtered Cu K α radiation. The morphology and particle size of the products were examined by field-emission scanning electron microscopy (FESEM) (Nova NanoSEM 230, FEI Corp.). High-resolution transmission electron microscopy (HRTEM) observation was carried out on a FEI Tecnai G2 F20 instrument operated at an accelerating voltage of 200 kV. The UV-vis diffuse reflectance spectra (DRS) were collected on a Varian Cary 500 spectrometer using BaSO₄ as a reference. N₂ adsorption-desorption measurements were conducted at 77 K on a Micromeritics ASAP2020 analyzer. Specific surface areas were determined by the Brunauer-Emmett-Teller (BET) method. Photoluminescence (PL) spectra were recorded on an Edinburgh FL/FS900 spectrophotometer. Electron paramagnetic resonance (EPR) signals were collected by a Bruker model A300 spectrometer (Bruker Instruments, Inc.) with the settings of center field (3512.48 G), microwave frequency (9.86

GHz), and power (6.35 mW). The photoelectrochemical experiment was measured using a CHI-660D electrochemical workstation filled with 0.1 M of Na₂SO₄ electrolyte (30 mL). The 60 different BiVO₄ samples were deposited as a film form on a 5 mm × 5 mm ITO conductive glass that served as the working electrode. A Pt plate and an Ag/AgCl electrode were used as the counter electrode and reference electrode, respectively.

2.3 Tests of photocatalytic activity

RhB, a typical fluorone dye, was also selected as a model contaminant in the photocatalytic experiment. A 500 W halogen lamp (Philips Electronics) was used as illuminating source and placed in a cylindrical glass vessel in which cold water was circulating to avoid overheating. The system was cooled by using a fan to maintain at 25 °C. Two cutoff filters were equipped to completely remove any radiation below 420 nm, ensuring the BiVO₄/RhB aqueous mixture was irradiated only by visible light (420 nm < λ < 800 nm). 0.08 g of photocatalyst was suspended in 80 mL of RhB aqueous solution (1 × 10⁻⁵ mol/L) and stirred for 2h in dark to ensure adsorption/desorption equilibrium had been reached. During irradiation, a 3 mL of the suspension was sampled at given time intervals, which was then centrifuged to remove the photocatalyst. A Varian Cary 50 Scan UV-vis spectrophotometer was used to record the concentration changes of the resulting degraded RhB solution. The percentage of degradation is reported as C/C₀. C is the absorption of RhB at each irradiated time interval of the maximum peak of the absorption spectrum at wavelength of 554 nm. And C₀ is the absorption of the initial concentration when adsorption/desorption equilibrium is achieved.

3. Results and discussion

3.1 Characterizations of catalysts

Fig. 1 shows the XRD patterns of the as-prepared samples as a function of hydrothermal reaction time and Bi/V molar ratios. When the Bi/V molar ratio was 4/1 and the synthesis temperature was 180 °C, the tetragonal zircon structure BiVO₄ (z-t BiVO₄, JCPDS No. 14-0133) was the dominant phase (Fig. 1a). As the reaction time increased to 48 h and 72 h, the peak at 28.8° for the monoclinic scheelite structure BiVO₄ (s-m BiVO₄, JCPDS No. 14-0688) appeared, indicating that the samples were mixture of z-t BiVO₄ and s-m BiVO₄ (z-t & s-m BiVO₄). Particularly, when the reaction time was 48 h, the sharp and narrow diffraction peaks indicated a high crystallinity of z-t BiVO₄. Thus, under the immobilization conditions (180 °C, 48 h), the influence of the Bi/V molar ratio on the phase structure of BiVO₄ was investigated. As it can be seen in Fig. 1b, when the Bi/V molar ratio was 1/1 and 2/1, the XRD patterns of the samples were corresponding to the s-m BiVO₄. With the increasing of the Bi/V molar ratio, the z-t BiVO₄ was the dominant phase, and a small amount of s-m BiVO₄ was detected. The effect of reaction temperature on the phase compositions of BiVO₄ was also studied (Fig. S1 in Supplementary Information). When the reaction temperature was below 180 °C, the samples were in z-t BiVO₄ structure without any impurity phase. However, with further increase of reaction temperature up to 200 °C, all the z-t BiVO₄ transformed into the s-m BiVO₄. The XRD results indicated that lower Bi/V molar ratio, longer reaction time and

higher temperature favored the formation of s-m BiVO_4 . Moreover, the z-t & s-m heterophase BiVO_4 could be readily

prepared by adjusting the Bi/V molar ratio and hydrothermal reaction time.

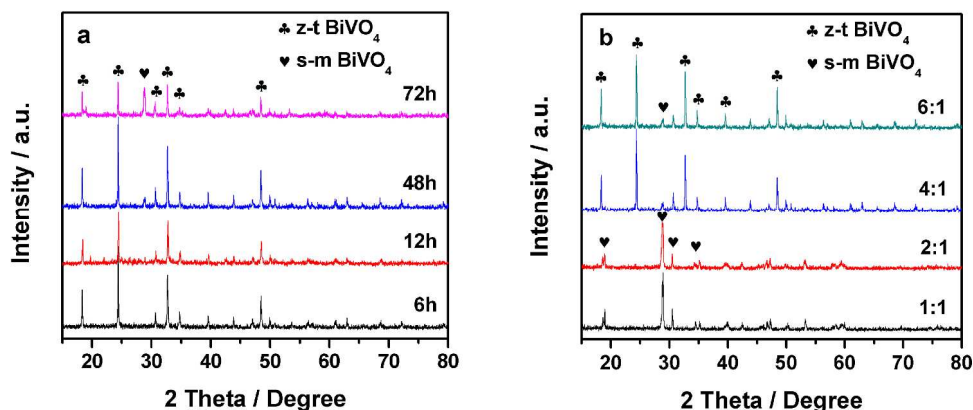


Fig.1 XRD patterns of BiVO_4 synthesized at 180°C for different holding time with Bi/V molar ratio of 4/1 (a) and BiVO_4 synthesized at 180°C for 48 h with different Bi/V molar ratios (b).

The morphologies of the as-prepared BiVO_4 samples were examined by FESEM technique. Fig. 2 presents FESEM images of the BiVO_4 samples with Bi/V molar ratio of 4/1 prepared at 180°C for different holding time. When the reaction time was 6 h, relatively complete BiVO_4 microspheres with average diameters of about 3-5 μm formed (Fig. 2a), and the microspheres were composed of a large quantity of particles. As the reaction time extended to 12 h and 48 h, more and more microspheres collapsed, as shown in Fig. 2b and Fig. 2c. When the reaction time increased to 72 h, all the microspheres collapsed into irregular particles (Fig. 2d).

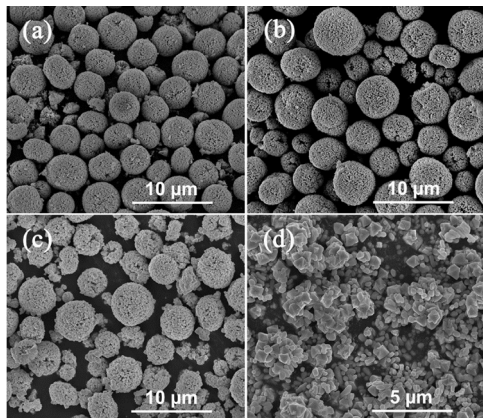


Fig.2 FESEM images of BiVO_4 samples with Bi/V molar ratio of 4/1 prepared at 180°C for different holding time: (a) 6 h; (b) 12 h; (c) 48 h; (d) 72 h.

Fig. 3 shows the morphologies of as-synthesized BiVO_4 prepared at 180°C for 48 h with different Bi/V molar ratios. When the Bi/V molar ratio were 1/1 and 2/1, the s-m BiVO_4 samples were composed of polyhedron particles with a size of ca. 1 μm , and the aggregation among particles was obvious (Fig. 3a, b). The products with Bi/V molar ratio of 4/1 and 6/1 were composed of a large quantity of microspheres with an average diameter of about 4-6 μm (Fig. 3c, d). The influence of hydrothermal temperature on the morphology was also investigated. When the product was treated at lower temperature, immature microspheres were observed which adhered with each

other (Fig. S2a). As the temperature increased to 200°C , the spheres collapsed and lots of BiVO_4 particles formed (Fig. S2b). From these figures, we can come to a conclusion that the Bi/V molar ratio and hydrothermal time have significant effects on the morphologies of the samples. Fig. 4 shows the schematic illustration of various synthesis conditions and their corresponding structures.

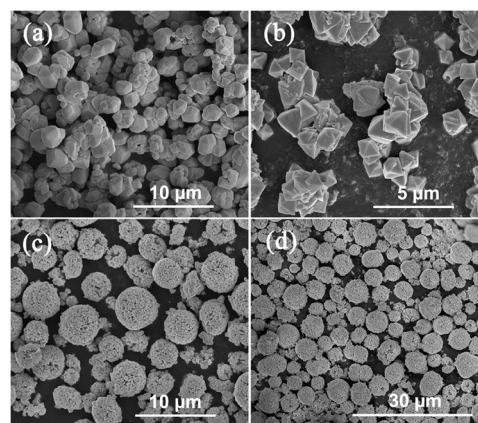


Fig.3 FESEM images of BiVO_4 samples prepared at 180°C for 48 h with different Bi/V molar ratios: (a) 1/1; (b) 2/1; (c) 4/1; (d) 6/1.

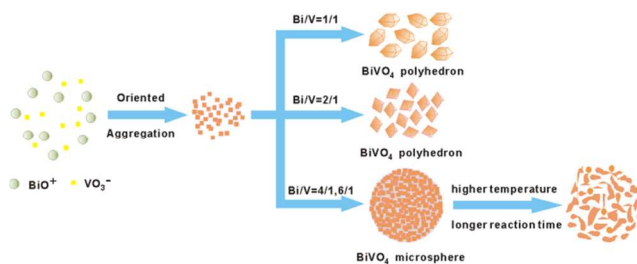


Fig.4 Schematic illustration of the synthesis conditions and their morphological results.

Fig. 5 shows the TEM images of the BiVO_4 sample prepared at 180°C for 48 h with Bi/V molar ratio of 4/1. Part a of Fig. 5 presented an individual microsphere with a solid circle, in accordance with the corresponding FESEM image (Fig. 2c). Part b of Fig. 5 was the enlarged HRTEM image of the area marked

by a red square in part a of Fig. 5. Obviously, two different kinds of lattice fringes were clearly presented. The distinct fringe of $d = 0.467$ nm matched that of the (011) crystallographic plane of s-m BiVO₄, while the fringe with interplanar spacing 0.258 nm was corresponding to (220) crystallographic plane of z-t BiVO₄. The above results further indicated that the as-synthesized sample was composed of z-t BiVO₄ and s-m BiVO₄, which was consistent with the results of XRD.

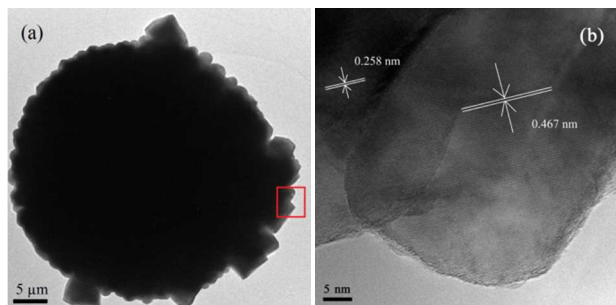


Fig. 5 TEM and HRTEM images of BiVO₄ sample with Bi/V molar ratio of 4/1 prepared at 180 °C for 48 h.

Fig. 6 displays the UV-vis DRS of the as-obtained BiVO₄ products. It can be seen that all the BiVO₄ products exhibited strong absorption in the visible range. From Fig. 6a, the light absorption exhibited red-shifts upon the increasing reaction time.

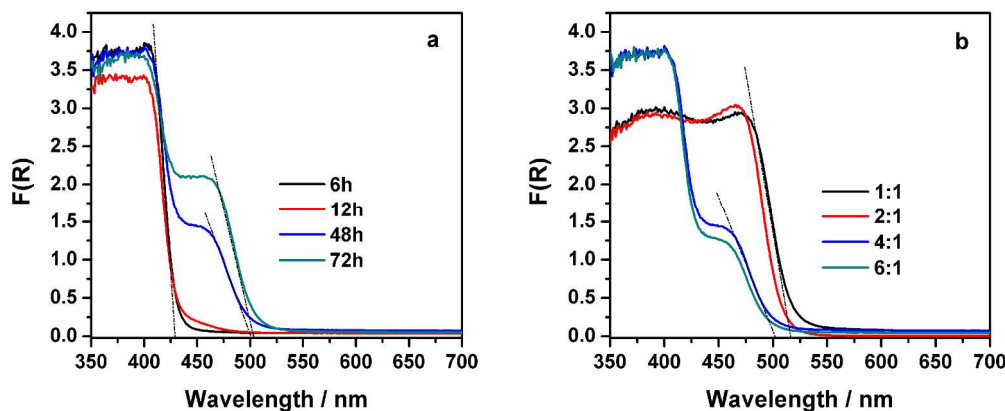


Fig. 6 DRS of BiVO₄ samples with Bi/V molar ratio of 4/1 prepared at 180 °C for different holding time (a) and prepared at 180 °C for 48 h with different Bi/V molar ratios (b).

3.2 Photocatalytic degradation of RhB

The photocatalytic activities of the samples were mainly evaluated by measuring the photodegradation of RhB aqueous solution under visible light irradiation, as shown in Fig. 7. There was almost no decolorization in the solution without any catalysts. The absorption-desorption equilibrium was established after 2 h in dark absorption for BiVO₄ photocatalysts. After 6 h of irradiation time, the BiVO₄ sample prepared at 180 °C for 48 h exhibited the best activity, corresponding to the degradation ratio of about 97.7% after 6 h of visible light irradiation. It may result in the fact that when the reaction time was longer, the BiVO₄ microsphere collapsed and the formed BiVO₄ particles were agglomerated and not well dispersed. Fig. 7b displays the concentration changes of RhB as a function of irradiation time in the presence of BiVO₄ samples prepared at 180 °C for 48 h with

As for the BiVO₄ sample synthesized for 6 h, the absorption intensity in the visible region was obviously lower than that of the other three samples, and the λ_{ab} ended at 429 nm with band gap of 2.89 eV. When the reaction time was 48 h, the λ_{ab} was estimated to be about 501 nm, corresponding to the band gap energy of 2.48 eV. With the reaction time increased to 72 h, the absorption intensity in the visible region was higher than that of the other samples. Varying the Bi/V molar ratio from 1/1 to 6/1, the light absorption exhibited blue-shifts (Fig. 6b). When the Bi/V molar ratio was 1/1, the XRD pattern was proved to be the s-m BiVO₄ phase. It showed the strongest visible-light-response among the four tested samples, and its absorption onset could be extended to 517 nm, corresponding to the band gap of 2.4 eV. When Bi/V molar ratio was 6/1, its absorption in the visible-light region was the weakest, corresponding to the highest band gap. The steep shape of the above two spectra indicates that their absorption in the visible-light region is due to the band gap transition.^{26,27} Moreover, Fig. S3 shows that the light absorption exhibited red-shifts upon the increasing reaction temperature. When the treatment time was increased to 200 °C, the absorption onset dropped to 507 nm, corresponding to the band gap of 2.45 eV. The difference in the bandgaps of the as-prepared samples will make them show different photocatalytic activity under visible light irradiation.

different Bi/V molar ratios. It is clear the RhB removal value over BiVO₄ with the Bi/V molar ratio of 1/1 was the lowest, and only 64.4% of RhB was decomposed after 6 h of visible light irradiation. On the contrary, the samples with the Bi/V molar ratio of 2/1 and 6/1 degraded 78.2% and 94.1% of RhB, respectively. In addition, the effect of hydrothermal temperature on the photocatalytic activity was also investigated (Fig. S4). The sample synthesized at different temperature exhibited different activities, and the catalyst prepared at 180 °C revealed the best activity. Based on the above results, the differences in the photocatalytic activity may be caused by the morphology and BET specific surface area of BiVO₄. The related information was summarized as shown in Table 1. According to $V_{\text{monoclinic}} = I_{\text{monoclinic}(121)} / (I_{\text{monoclinic}(121)} + I_{\text{tetragonal}(200)})$,²⁸ the percentage of the monoclinic phase was calculated.

Cite this: DOI: 10.1039/c0xx00000x

www.rsc.org/xxxxxx

ARTICLE TYPE

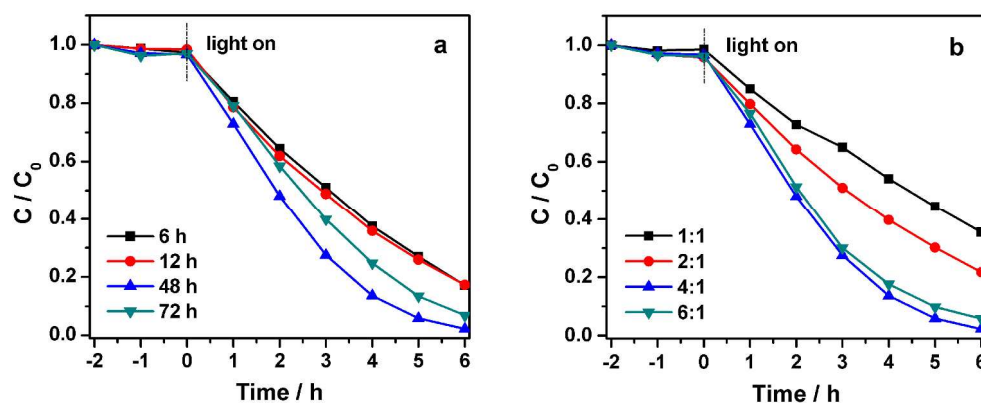


Fig.7 Degradation curves of RhB over the BiVO_4 samples with Bi/V molar ratio of 4:1 prepared at 180 °C for holding different time (a), prepared at 180 °C for 48 h with different Bi/V molar ratios (b).

Table 1 Crystal structures and RhB degradation ratio of BiVO_4 samples obtained under different preparation conditions.

Bi/V	Temperature (°C)	Time (h)	mon./(mon.+tetr.) ^a	BET surface area ($\text{m}^2 \cdot \text{g}^{-1}$)	RhB degradation ratio (%)
4/1 ^b	180	6	0	2.42	82.9
4/1	180	12	0	2.02	82.7
1/1 ^c	180	48	1	0.57	64.4
2/1	180	48	1	0.87	78.2
4/1 ^d	180	48	0.1	2.62	97.7
4/1	120	48	0.06	1.63	67.6
4/1	200	48	1	0.94	84.7
6/1	180	48	0.11	2.58	94.1
4/1	180	72	0.44	1.04	93.1

^a mon./(mon.+tetr.) denotes the percentage of the monoclinic phase in the heterophase. ^b The BiVO_4 sample is abbreviated as z-t BiVO_4 . ^c The BiVO_4 sample is abbreviated as s-m BiVO_4 . ^d The BiVO_4 sample is abbreviated as z-t & s-m BiVO_4 .

3.3 Photocatalytic activity discussions

To clarify the reasons of the enhanced photocatalytic activity, we detected the involved active species forming in the photocatalytic reaction under visible light irradiation. In order to simplify the experiment, the above three BiVO_4 samples (b, c, d in Table 1) were selected as models for the further study. To recognize the formation of hydroxyl radicals ($\cdot\text{OH}$), the TA-PL probing technique was firstly used in the BiVO_4 systems.²⁹ In the BiVO_4/TA system, when irradiated with visible light, 2-hydroxyl-terephthalic acid is generated, which is captured by terephthalic acid (TA) and performs a strong fluorescence characteristic (Fig. 8). So monitoring the fluorescence intensity changes of 2-hydroxyl-terephthalic acid in BiVO_4/TA suspension, we can indirectly detect the generation of hydroxyl radicals. Fig.8 shows the $\cdot\text{OH}$ -trapping PL spectra of suspensions containing different photocatalysts and TA. As we can see, the fluorescence intensity increased in different degrees with the irradiation time within 6 h. It can be concluded that hydroxyl radicals were indeed generated in the BiVO_4 suspension under visible light irradiation. The z-t & s-m BiVO_4 which presented the best photocatalytic activity generated the most hydroxyl radicals. And the general trend of hydroxyl radical generation was in accordance with that of RhB

degradation, suggesting hydroxyl radical were indeed generated on BiVO_4 under visible light irradiation as one of the active species.

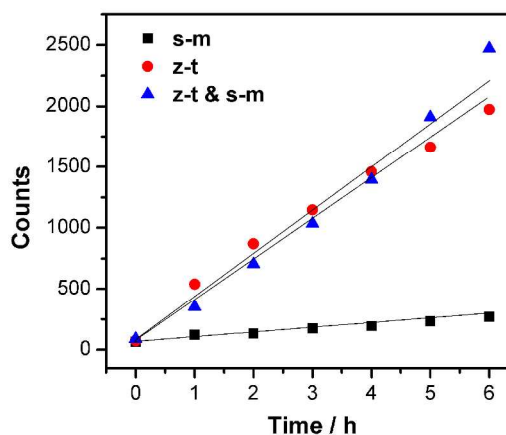


Fig.8 The comparison plot of temporal changes in $\cdot\text{OH}$ -trapping PL spectra of s-m BiVO_4 , z-t BiVO_4 and z-t & s-m BiVO_4 under visible light irradiation.

The spin trapping EPR technique was also used to detect the

reactive oxygen species generated in the heterophase photocatalytic process. Fig.9 shows the spin-trapping EPR spectra of z-t & s-m BiVO₄. It could be seen that there was no obvious signal corresponding to DMPO-•OH and DMPO-O₂•⁻ in dark. However, under visible light irradiation, four characteristic peaks of DMPO-•OH could be obviously observed in the suspension. Similarly, only under visible light irradiation, the six characteristic peaks corresponding to the spin-adducts DMPO-O₂•⁻ could be observed in the methanol solvent. On the basis of the above characterization, it indicated that •OH and O₂•⁻ species existed and participated in the degradation process.

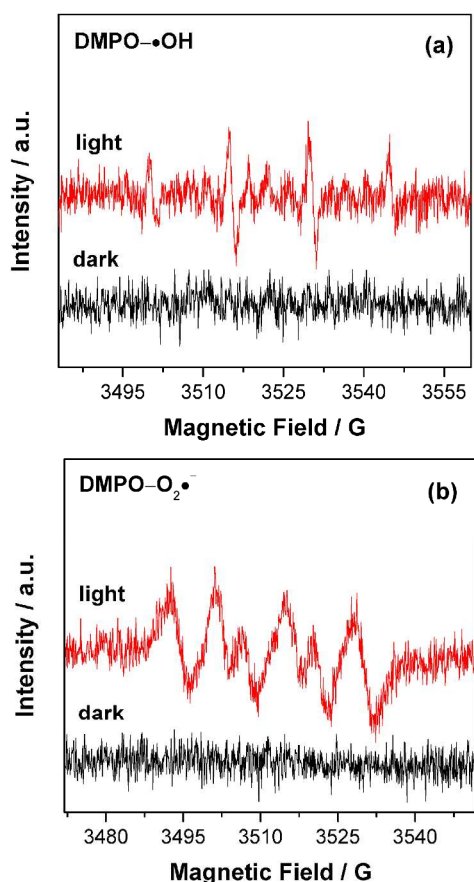


Fig.9 EPR spectral features of z-t & s-m BiVO₄ in aqueous dispersion for DMPO-•OH (a) and in methanol dispersion for DMPO-O₂•⁻ (b) (420 nm λ <math>< 800</math> nm).

To further evaluate the role of these active species such as electrons/holes, •OH and O₂•⁻, some additional conditions that affected the generation of active species were applied in the degradation process.^{30,31} Fig. 10 shows the photocatalytic activity of z-t & s-m BiVO₄ towards the degradation of RhB under different conditions. Without the addition of the scavengers, the photocatalytic degradation rate of RhB is 97.7% after 6 h of visible irradiation (the original curve). Ammonium oxalate (AO) is an effective scavenger of holes.³² After 0.1 g of AO was added to the reaction system, the degradation ratio of RhB was decreased to 75%. The addition of AO inhibited the photocatalytic degradation process. There are two reasons: one is that the photogenerated hole in heterophase BiVO₄ would activate some unsaturated organic pollutants, resulting in

subsequent decomposition. Another is the presence of AO aborted the generation of active species and high mobility of charge carriers of the circulatory system which seriously inhibits the photocatalytic degradation process. Tert-butyl alcohol (TBA), as a scavenger for •OH, was also added in the system. From the figure, in the presence of 2 mL of TBA, the degradation ratio of RhB was decreased to 88% after 6 h of irradiation. So, the RhB oxidation was driven by the contribution of •OH radicals to a lesser extent. It is worth noting that the condition after adding the benzoquinone (BQ) was quite different. BQ has the ability to trap O₂•⁻ by a simple electron transfer mechanism.^{33,34} With the addition of 1 mg of BQ, the rate for degradation of RhB over z-t & s-m BiVO₄ was dramatically decreased and only about 15% of RhB was degraded.

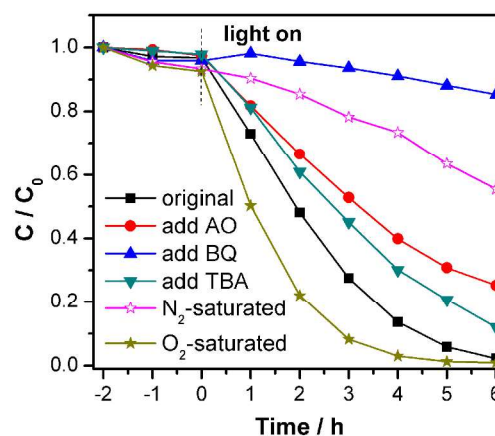


Fig.10 Photocatalytic degradation of RhB over z-t & s-m BiVO₄ under different conditions with exposure to visible light: original, adding AO, adding BQ, adding TBA, N₂-saturated and O₂-saturated.

Moreover, dissolved O₂ as an efficient electron scavenger and an important source of O₂•⁻ was excluded under flowing N₂ gas (flow rate: 50 mL·min⁻¹) in the degradation process. After the light irradiation, the photocatalytic conversion ratio was decreased to 44%. And by bubbling O₂ gas (flow rate: 50 mL·min⁻¹), the dissolved O₂ could be increased and the corresponding degradation ratio was increased. Therefore, the electrons or the active species generated by electrons play an important role in the heterophase photocatalytic reaction. A combination of the results of EPR and the addition of BQ indicates that O₂•⁻ played a very important role in the photocatalytic process. And the holes and •OH were the subordinate factors. However, we can still detect the signal of •OH on the surface of heterophase BiVO₄ by TA-PL and EPR techniques. To sum up, through the comparison, we can conclude that the RhB oxidation was driven mainly by the participation of O₂•⁻ and holes, and to a lesser extent by the contribution of •OH. In addition, photoelectrochemical technique was applied to study the charge transfer and separation of photogenerated electron-hole pairs over the photocatalyst/electrolyte interfaces. The photocurrent density-time (I-t) profiles without any bias electrode potential were given as shown in Fig. 11a. When visible light source was turned on or off, the instantaneous photocurrent of pure s-m BiVO₄ and z-t BiVO₄ were in a small degree, which was corresponding to the weak photodegradation of organic pollutants. The photocurrent resulted from the photogenerated

electron/hole pairs of excited BiVO_4 under visible light irradiation. Obviously, the photocurrent of z-t & s-m BiVO_4 was greatly increased at given time intervals (40 s). Furthermore, electrochemical impedance spectroscopy (EIS) was also used to investigate the charge transfer resistance and the separation efficiency of photogenerated charge. Fig. 11b shows EIS response of s-m/z-t BiVO_4/FTO films and z-t & s-m BiVO_4/FTO film under visible-light irradiation. The radius of the arc on the EIS Nyquist plot reflects the reaction rate occurring at the surface of electrode. Obviously, the arc radius on EIS Nyquist plot of z-t & s-m BiVO_4/FTO film was smaller than that of z-t BiVO_4/FTO film and s-m BiVO_4/FTO film samples. It indicates that z-t & s-m BiVO_4 has lower resistance than that of pure s-m BiVO_4 and z-t BiVO_4 . The results of photoelectrochemical tests

indicated that the presence of heterophase was capable of improving separation efficiency and effectively inhibit the electron-hole pair recombination. Thus, the z-t & s-m heterophase BiVO_4 had a higher photocatalytic performance compared with the pure s-m BiVO_4 and z-t BiVO_4 . In conclusion, the RhB oxidation over z-t & s-m heterophase BiVO_4 was driven mainly by the participation of electrons and $\text{O}_2^{\bullet-}$ radicals, and to a lesser extent by the contributions of holes and $\bullet\text{OH}$ radicals. These radicals attacked the RhB molecules adsorbed on the surface of catalyst, leading to the efficiently photocatalytic oxidation of RhB. Our studies open a door toward facile improvement in the efficiency of BiVO_4 , promoting its great potential in environmental pollutant cleanup applications.

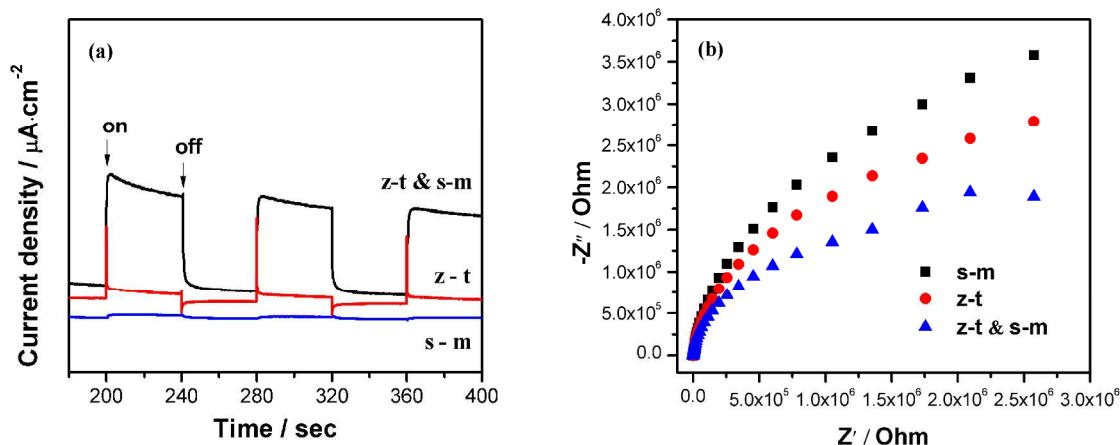


Fig.11 (a) Comparison of transient photocurrent responses and (b) EIS Nyquist plots of the s-m BiVO_4 , z-t BiVO_4 and z-t & s-m BiVO_4 under visible light irradiation ($420 \text{ nm} < \lambda < 800 \text{ nm}$, $[\text{Na}_2\text{SO}_4] = 0.1 \text{ M}$).

4. Conclusions

In summary, BiVO_4 microsphere with tetragonal-zircon/monoclinic-scheelite heterophase, had been successfully synthesized via a one-pot template-free hydrothermal method. The formation of heterophase had a significant influence on the microstructures and photodegradation efficiency of the photocatalyst. Benefiting from the high surface area and extended absorption in the visible light region, the heterophase BiVO_4 sample exhibited the highest photocatalytic activity with 97.7% of RhB degraded, remarkably superior to the pure monoclinic-scheelite BiVO_4 and tetragonal-zircon BiVO_4 . Such an improved photocatalytic activity was ascribed to the most effectively separation efficiency of photogenerated carriers generated in the heterophase BiVO_4 system, as evidenced by the electrochemical measurement. $\bullet\text{OH}$ and $\text{O}_2^{\bullet-}$ had been detected in the suspension of heterophase BiVO_4 microsphere by the TA-PL and EPR techniques. Based on free-radical scavenging and N_2/O_2 -purging experiments, the decomposition of RhB was driven mainly by the participation of $\text{O}_2^{\bullet-}$ and a lesser extent by the participation of holes and $\bullet\text{OH}$.

Acknowledgements

The authors gratefully acknowledge financial support for this

research from the National Natural Science Foundation of China (21173047, 21373049 and 31260400), the Natural Science Foundation of Jiangxi (20142BAB213012, 20122BAB214003), Science and Technology Support Project of Jiangxi (20142BBE50007), Scientific Research Foundation of Jiangxi Academy of Sciences, and Open Project from State Key Laboratory of Photocatalysis on Energy and Environment of Fuzhou University.

Notes and references

- ^aResearch Institute of Applied Chemistry, Jiangxi Academy of Sciences, Nanchang, Jiangxi, 330096, P. R. China.
- ^bResearch Institute of Photocatalysis, State Key Laboratory of Photocatalysis on Energy and Environment, Fuzhou University, Fuzhou, 350002, P. R. China. Fax: +86-591-83779256; Tel: +86-591-83779256; E-mail: dzli@fzu.edu.cn.
- M. R. Hoffmann, S. T. Martin, W. Y. Choi and D. W. Bahnemann, *Chem. Rev.*, 1995, **95**, 69.
- C. C. Chen, W. H. Ma and J. C. Zhao, *Chem. Soc. Rev.*, 2010, **39**, 4206.
- H. H. Chen, C. E. Nanayakkara and V. H. Grassian, *Chem. Rev.*, 2012, **112**, 5919.
- M. Nolan, *Chem. Commun.*, 2011, **47**, 8617.
- W. J. Zhou, Z. Y. Yin, Y. P. Du, X. Huang, Z. Y. Zeng, Z. X. Fan, H. Liu, J. Y. Wang and H. Zhang, *Small*, 2013, **9**, 140.

- 6 Z. G. Yi, J. H. Ye, N. Kikugawa, T. Kako, S. X. Ouyang, H. Stuart
Williams, H. Yang, J. Y. Cao, W. J. Luo, Z. S. Li, Y. Liu and R. L.
Withers, *Nat. Mater.*, 2010, **9**, 559.
- 7 Y. H. He, D. Z. Li, J. Chen, Y. Shao, J. J. Xian, X. Z. Zheng and P.
Wang, *RSC Adv.*, 2014, **4**, 1266.
- 8 A. Kudo, K. Omori and H. Kato, *J. Am. Chem. Soc.*, 1999, **121**,
11459.
- 9 Y. Park, K. J. McDonald and K. S. Choi, *Chem. Soc. Rev.*, 2013, **42**,
2321.
- 10 C. Yin, S. M. Zhu, Z. X. Chen, W. Zhang, J. J. Gu and D. Zhang, *J.*
Mater. Chem. A, 2013, **1**, 8367.
- 11 X. F. Zhang, Y. B. Zhang, X. Quan and S. Chen, *J. Hazard. Mater.*,
2009, **167**, 911.
- 12 M. C. Long, W. M. Cai, J. Cai, B. X. Zhou, X. Y. Chai and Y. H. Wu,
15 *J. Phys. Chem. B*, 2006, **110**, 20211.
- 13 Y. Hu, D. Z. Li, Y. Zheng, W. Chen, Y. H. He, Y. Shao, X. Z. Fu and
G. C. Xiao, *Appl. Catal. B: Environ.*, 2011, **104**, 30.
- 14 Z. Q. He, Y. Q. Shi, C. Gao, L. N. Wen, J. M. Chen and S. Song, *J.*
Phys. Chem. C, 2014, **118**, 389.
- 20 15 M. D. Han, T. Sun, P. Y. Tan, X. F. Chen and O. K. Tan, *RSC Adv.*,
2013, **3**, 24964.
- 16 W. D. Shi, Y. Yan and X. Yan, *Chem. Eng. J.*, 2013, **215**, 740.
- 17 G. C. Xi and J. H. Ye, *Chem. Commun.*, 2010, **46**, 1893.
- 18 R. G. Li, F. X. Zhang, D. E. Wang, J. X. Yang, M. R. Li, J. Zhu, X.
Zhou, H. X. Han and C. Li, *Nat. Commu.* 2013, **4**, 1432.
- 25 19 S. Tokunaga, H. Kato and A. Kudo, *Chem. Mater.*, 2001, **13**, 4624.
- 20 J. Zhang, Q. Xu, Z. C. Feng, M. J. Li and C. Li, *Angew. Chem. Int.*
Ed., 2008, **47**, 1766.
- 21 X. Wang, Q. Xu, M. R. Li, S. Shen, X. L. Wang, Y. C. Wang, Z. C.
Feng, J. Y. Shi, H. X. Han and C. Li, *Angew. Chem. Int. Ed.*, 2012,
30 **51**, 13089.
- 22 K. Pan, Y. Z. Dong, W. Zhou, G. F. Wang, Q. J. Pan, Y. Yuan, X. H.
Miao and G. H. Tian, *Electrochim. Acta*, 2013, **88**, 263.
- 23 Y. X. Liu, Z. L. Wang, W. D. Wang and W. X. Huang, *J. Catal.*,
35 2014, **310**, 16.
- 24 Z. W. Wei, X. C. Wei, S. Y. Wang and D. Y. He, *Mater. Lett.*, 2014,
118, 107.
- 25 H. M. Fan, T. F. Jiang, H. Y. Li, D. J. Wang, L. L. Wang, J. L. Zhai,
D. Q. He, P. Wang and T. F. Xie, *J. Phys. Chem. C*, 2012, **116**, 2425.
- 40 26 A. P. Zhang, J. Z. Zhang, N. Y. Cui, X. Y. Tie, Y. W. An and L. J. Li,
J. Mol. Catal. A: Chem., 2009, **304**, 28-32.
- 27 Y. N. Guo, X. Yang, F. Y. Ma, K. X. Li, L. Xu, X. Yuan and Y. H.
Guo, *Appl. Surf. Sci.*, 2010, **256**, 2215-2222.
- 28 A. K. Bhattacharya, K. K. Mallick and A. Hartridge, *Mater. Lett.*,
45 1997, **30**, 7.
- 29 J. C. Barreto, G. S. Smith, N. H. P. Strobel, P. A. Mcquillin and T. A.
Miller, *Life Sci.*, 1995, **56**, 89.
- 30 W. J. Li, D. Z. Li, Y. M. Lin, P. X. Wang, W. Chen, X. Z. Fu and Y.
Shao, *J. Phys. Chem. C*, 2012, **116**, 3552.
- 50 31 W. J. Li, D. Z. Li, J. X. Wang, Y. Shao, J. M. You and F. Teng, *J.*
Mol. Catal. A: Chem., 2013, **380**, 10.
- 32 H. Kominami, A. Furusho, S. Murakami, H. Inoue, Y. Kera and B.
Ohtani, *Catal. Lett.*, 2001, **76**, 31.
- 33 M. Styliidi, D. I. Kondarides and X. E. Verykios, *Appl. Catal. B:*
55 *Environ.*, 2004, **47**, 189.
- 34 P. Raja, A. Bozzi, H. Mansilla, J. Kiwi, *J. Photochem. Photobiol. A*,
2005, **169**, 271.

Graphical abstract

Well-defined BiVO_4 microsphere with tetragonal-zircon/monoclinic-scheelite heterophase was synthesized by a facile hydrothermal route, without the use of any template or organic surfactant. XRD and HRTEM characterizations confirmed that the formation of heterophase structure, which had a significant influence on the microstructures and photodegradation efficiency. The heterophase BiVO_4 sample exhibited the highest photocatalytic activity with 97.7% of RhB was degraded, remarkably superior to the pure monoclinic-scheelite BiVO_4 and tetragonal-zircon BiVO_4 . Such an improved photocatalytic activity was ascribed to the most effectively separation efficiency of photogenerated carriers generated in the heterophase BiVO_4 system, as evidenced by the electrochemical measurement. The main active oxygen free radical that was mostly responsible for the degradation had been tested and the mechanism was discussed in detail. The present study proves that designing heterophase structure is a feasible approach for developing highly visible-light-active semiconductor photocatalysts.

